Hindawi
Journal of Nanomaterials
Volume 2017, Article ID 8305439, 7 pages
https://doi.org/10.1155/2017/8305439

Research Article

Fabrication of a Large-Area Superhydrophobic SiO_2 Nanorod Structured Surface Using Glancing Angle Deposition

Xun Lu,[1] Seok-min Kim,[1] and Seong Jun Seo[2]

[1]*School of Mechanical Engineering, Chung-Ang University, Seoul 06974, Republic of Korea*
[2]*Department of Dermatology, Chung-Ang University Hospital, Seoul 06973, Republic of Korea*

Correspondence should be addressed to Seok-min Kim; smkim@cau.ac.kr and Seong Jun Seo; drseo@cau.ac.kr

Received 24 April 2017; Accepted 21 August 2017; Published 16 October 2017

Academic Editor: Weilu Gao

A glancing angle deposition (GLAD) technique was used to generate SiO_2 nanorods on a glass substrate to fabricate a low-cost superhydrophobic functional nanostructured surface. GLAD-deposited SiO_2 nanorod structures were fabricated using various deposition rates, substrate rotating speeds, oblique angles, and deposition times to analyze the effects of processing conditions on the characteristics of the fabricated functional nanostructures. The wettability of the surface was measured after surface modification with a self-assembled monolayer (SAM). The measured water contact angles were primarily affected by substrate rotation speed and oblique angle because the surface fraction of the GLAD nanostructure was mainly affected by these parameters. A maximum contact angle of 157° was obtained from the GLAD sample fabricated at a rotation speed of 5 rpm and an oblique angle of 87°. Although the deposition thickness (height of the nanorods) was not a dominant factor for determining the wettability, we selected a deposition thickness of 260 nm as the optimum processing condition based on the measured optical transmittance of the samples because optically transparent films can serve as superhydrophobic functional nanostructures for optical applications.

1. Introduction

Optically transparent multifunctional surfaces play an important role in photovoltaic applications for improving or maintaining system performance. Incident solar energy on the photovoltaic modules is decreased through both surface contamination on the outdoor panels and optical reflection at the interface between the air and packaging glass. It is therefore important to develop optically transparent self-cleaning surfaces with low optical reflectance. In practical operating conditions for solar cells, surface contamination of the photovoltaic modules by dust accumulation is always possible. It has been reported that the accumulation of dust on the window of a solar cell causes degradation in the solar cell efficiency [1, 2]. It is commonly claimed that superhydrophobic surfaces can provide self-cleaning windows in solar cell applications [3, 4]. There are two main approaches that can be considered to increase surface hydrophobicity. One approach is to decrease the surface energy by modifying the surface chemistry, and the other is to create a geometrical structure with a material that has a low surface energy [5, 6]. Although chemical treatment of the surface is convenient, the maximum contact angle attainable on a flat surface with the lowest free energy coating is only 115.2°, as pointed out by Nakajima [7]. Also, since reflection loss is caused by a mismatch in refractive indices, it is not feasible to reduce the reflective optical loss by chemical modification. Higher contact angles can be easily obtained by changing the surface morphology with nanostructures. In addition, nanostructured surfaces both increase the contact angle and increase the optical transmittance due to gradient refractive index effects [8].

Various methods have been tried to create a nanostructured hydrophobic surface with antireflective properties including photolithography [9], chemical etching [10], and plasma enhanced chemical vapor deposition [11]. However, these techniques have limitations that make it difficult to fabricate well-controlled uniform nanostructures on large-area substrates at low cost, which is important for commercialization of superhydrophobic functional nanostructured surfaces. Although a polymer nanoimprinting technique has been proposed to fabricate well-controlled uniform

nanostructures on a large-area substrate at low cost [12], the imprinted nanostructure cannot guarantee long-term stability in an outdoor environment because the different thermal expansion coefficients of the substrate and imprinted layer might cause a delamination problem.

In this paper, we fabricated a SiO_2 nanorod structured superhydrophobic surface on a glass substrate using a glancing angle deposition (GLAD) technique. GLAD is an effective method of fabricating nanostructures on large areas with various materials at low cost, and the shape of a GLAD nanostructure can be easily controlled by changing the processing parameters. In previous reports, superhydrophobic [13, 14] and antireflection surfaces [15, 16] were fabricated using a GLAD technique, but these surfaces are limited as they cannot provide both characteristics at the same time. In this study, we fabricated superhydrophobic and antireflection surfaces using SiO_2 nanorod structures on a conventional glass substrate by employing the GLAD technique. SiO_2 nanorods with various surface morphologies were fabricated under various deposition rates, substrate rotation speeds, oblique angles, and deposition thicknesses to optimize the processing parameters of the GLAD process and maximize the hydrophobicity of the nanostructures. After an additional coating with a self-assembled monolayer (SAM) on the SiO_2 nanorods, water contact angles (WCAs) were measured and compared with that of the theoretical model. Finally, optimal processing parameters of the GLAD process were selected for maximizing water repellency and optical transmittance.

2. Experimental

2.1. Fabrication of the Functional Nanostructured Surface. GLAD is a physical vapor deposition process in which deposition flux is incident onto the substrate at a large oblique angle with respect to the surface normal (75°~90°) [17]. GLAD is a single-step fabrication process providing a columnar morphology using the "shadowing effect" and precise in-plain rotation of the substrate. At the early stage of the GLAD process, the deposited particles are randomly scattered and form island structures on the substrate. As the deposition proceeds, the initial nucleated islands act as shadowing centers, with the taller islands receiving more impinging particles than the shorter ones (shadowing effect). This competition causes the taller islands to grow into columns, resulting in the formation of nanorod structures [18–20]. In this study, SiO_2 nanorod structures were fabricated on a $3 \times 1\,\text{inch}^2$ glass slide substrate by the GLAD technique using an electron beam evaporator (Modified SEE-7, Ultech, Co., Ltd., Korea) equipped with a sample holder capable of oblique angle deposition and rotation speed control. Prior to the deposition process, the glass slide substrates were cleaned in a sonication bath using acetone, isopropyl alcohol (IPA), and deionized water for 15 min each. The cleaned substrates were dried with nitrogen gas and mounted on a substrate holder in an electron beam evaporator, and the evaporation chamber was pumped down using a cryopump supported by a mechanical pump until it reached a base pressure of 6.0×10^{-7} Torr. The vacuum pressure during the evaporation was less than 5.0×10^{-6} Torr, and the growth rate during the deposition was monitored by employing a quartz crystal microbalance positioned at an incidence angle normal to the vapor source. The distance between the evaporation source and the rotating substrate was 680 mm. SiO_2 pellets (RND Korea, 99.999%) were used as a source material for the nanorods. In each experiment, the GLAD SiO_2 nanorods were deposited on 2 glass slide substrates and a $1 \times 1\,\text{cm}^2$ silicon substrate. The GLAD structures on the glass slide substrates were used to measure the WCA and optical transmittance, and those on the silicon substrates were used for scanning electron microscopy (SEM) measurements. To examine the effects of surface morphology on WCA and optical transmittance, various SiO_2 nanorod structures were fabricated at deposition rates of 5 and 10 Å/s, substrate rotation speeds of 0.2 to 20 rpm, oblique angles of 82° to 87°, and deposition thicknesses of 260 to 500 nm. The surfaces of the fabricated SiO_2 nanostructures were modified by a silane self-assembled monolayer (SAM) coating to reduce the surface energy. The SAM coating was achieved by dipping the nanostructured glass slide into a 2% solution of dimethyldichlorosilane dissolved in octamethylcyclooctasilane.

2.2. Measurement and Analysis of WCA on the Functional Nanostructured Surface. To evaluate the effect of nanostructure morphology on the water repellent properties, WCA was measured using a drop dispensing method at room temperature. A microdropper was utilized to dispense 10 μL drops of distilled water droplets onto a sample. An imaging system was employed to capture a static contact angle image, and the contact angle was calculated by imaging processing. To obtain reliable WCA measurements, the WCAs were measured at four random places on each sample, and 2 samples fabricated under the same conditions were used for the measurement. The average values and standard deviation of 8 WCA measurements were used for the analysis.

To explain the relationship between WCA and the morphology of the SiO_2 nanostructure, the measured WCAs were compared with the values obtained from theoretical models, including the Wenzel model [21] and the Cassie-Baxter model [22]. In the Wenzel model, the water droplet penetrates into the nanostructured surface, and no air gap is trapped on the surface. Under this condition, the apparent WCA is described according to the following equation:

$$\cos\theta_w = r\cos\theta_0. \tag{1}$$

Here, θ_w is the theoretical WCA of the nanostructured surface according to the Wenzel model, θ_0 is the measured WCA of the flat surface, and r is the roughness factor, which is defined as the ratio of the actual surface area of the nanostructures to their horizontal projection. In the Cassie-Baxter model, the water droplet cannot penetrate into the nanostructured surface, and the air gap is trapped between the nanostructures and the water droplet. The apparent contact angle in this state is described by

$$\cos\theta_c = f\left(\cos\theta_0 + 1\right) - 1. \tag{2}$$

Here, θ_c is the theoretical WCA for the Cassie-Baxter model, and f is the ratio of the solid surface in contact

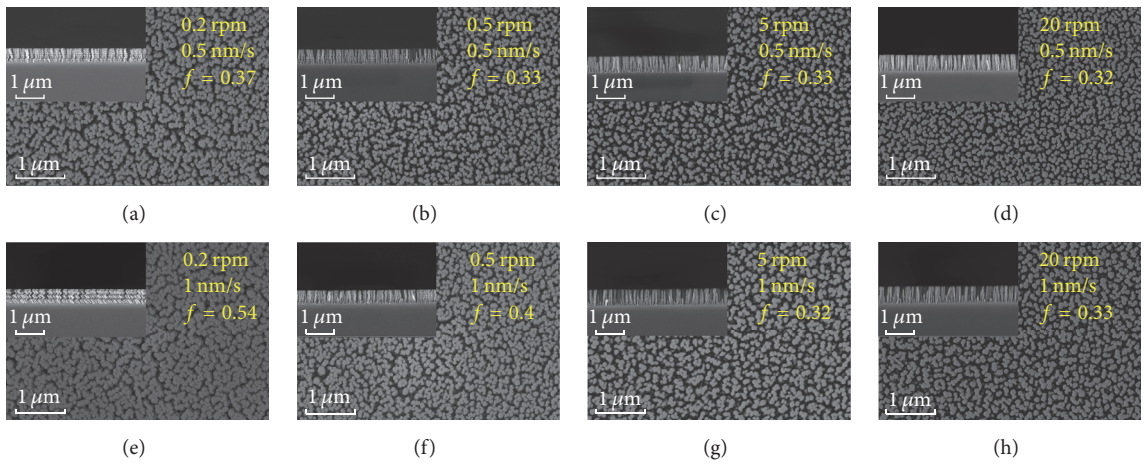

Figure 1: Top-view and cross-sectional view SEM images of GLAD SiO_2 nanorods fabricated at different deposition rates of 5 Å/s and 10 Å/s and different substrate rotation speeds of 0.2–20 rpm. The left top inset in each top-view SEM image is the cross-sectional view SEM image. The deposition rate, rotation speed, and the solid fraction are indicated on the right top of each SEM image.

with the water droplet (top area of the columnar structures) to the horizontal projection. The roughness factor (r) or solid fraction ratio (f) must be determined to calculate the predicted WCA for the Wenzel model or the Cassie-Baxter model. Since the GLAD nanorod structure can be simplified as a circular pedestal, the roughness factor (r) and solid fraction ratio (f) can be obtained using the following equations:

$$r = \frac{s + n(\pi dh)}{s} = 1 + \frac{n\pi dh}{s}, \qquad f = \frac{n\pi d^2}{4s}. \tag{3}$$

Here, d and h are the diameter and height of the nanorod, respectively; n is the number of nanorods per unit area, and s is the size of the unit area. Eventually, we developed two equations describing Wenzel and Cassie-Baxter angles as a function of nanorod geometry as described below:

$$\theta_w = \cos^{-1}\left[r\cos\theta_0\right], \qquad \theta_c = \cos^{-1}\left[f\left(\cos\theta_0 + 1\right) - 1\right]. \tag{4}$$

An image analysis technique was carried out using top-view SEM images to determine n, d, and s values. The grayscale SEM image was converted to a binary image by subtracting the background and adjusting the image contrast. The number (n) and diameter (d) of the nanorods were obtained from the converted binary top-view SEM images (white regions in the binary image were considered to be the top of a single nanorod), and the whole area of the SEM image was considered as the unit area (s). The height (h) of the nanorod was obtained from the cross-sectional SEM image.

In this research, the measured water contact angle (θ_0) of flat SiO_2 after SAM treatment was 103.9°. The Wenzel model loses its physical meaning when $\cos\theta_w$ is larger than 1, and $\cos\theta_w$ is larger than 1 when the r value is larger than 4.2. In this research, the calculated r value from the top-view SEM image of samples was larger than 5 except for the samples fabricated at an incident angle of 87°. In addition, the theoretical WCAs of the Wenzel model for the samples prepared at an incident angle of 87° did not match the experimental results. Therefore, the theoretical WCAs of this research were calculated using the Cassie-Baxter model.

2.3. Light Transmittance Measurement. Since the proposed SiO_2 nanorod structure can provide both hydrophobicity and antireflection characteristics, the light transmittance of the fabricated samples was also measured and analyzed. The optical transmittance of the fabricated SiO_2 nanorod structure on a glass slide substrate was measured using a spectrophotometer (UV-670 UV-Vis, Jasco Inc., USA) in the visible range.

3. Results and Discussion

3.1. Effects of Substrate Rotation Speed and Deposition Rate on WCA. To examine the effects of substrate rotation speed and deposition rate on the surface morphology and WCA, SiO_2 nanostructures were fabricated using a GLAD technique under the following conditions: substrate rotation from 0.2 to 20 rpm, deposition rates of 5 and 10 Å/s, a fixed thickness of 500 nm, and a fixed oblique angle of 82°. Figure 1 shows the SEM images of the fabricated GLAD SiO_2 nanostructures at different fabrication conditions, where the cross-sectional SEM images of each fabricated sample were inset in the top-view SEM image of the GLAD nanostructures. The rotation speed, deposition rate, and solid fraction ratio are indicated on the right top of the SEM images. In the cross-sectional SEM images, the nanorod shape changed from spiral to a straight vertical shape with increasing rotation speed. In the case of the spiral shape (Figures 1(a), 1(b), 1(e), and 1(f)), the f value and the diameter of the spiral structure decreased with increasing rotation speed and decreasing deposition rate. In the case of the vertical shape (Figures 1(c), 1(d), 1(g), and 1(h)),

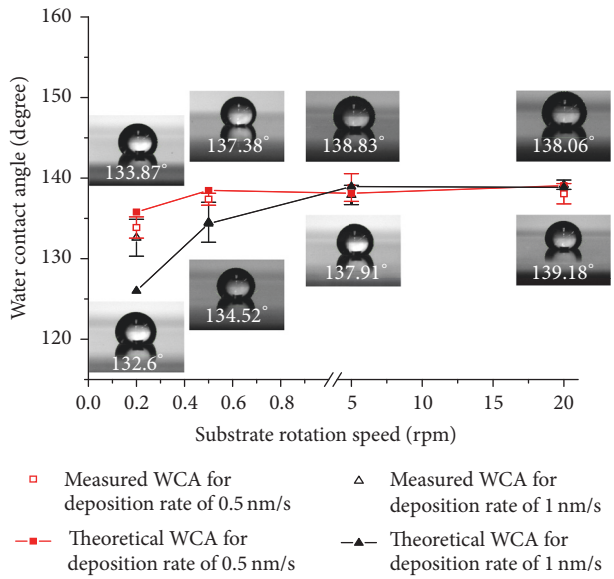

FIGURE 2: Effects of substrate rotation speed and deposition rate on the measured and theoretical (Cassie-Baxter model) WCAs of GLAD nanorod substrates.

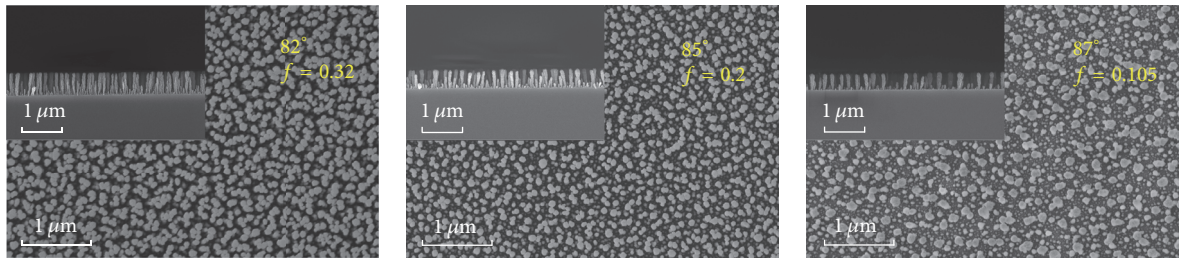

(a) (b) (c)

FIGURE 3: Top-view and cross-sectional view SEM images of fabricated GLAD SiO_2 nanorods at different deposition angles of 82, 85, and 87°.

however, the f value was not affected by rotation speed and deposition rate. In this research, the GLAD nanorod structure was considered to be a circular pedestal, and the diameter of the circular pedestal used to calculate the f value was obtained by image processing, in which the bright gray area of the top-view SEM image was considered to be the top of the cylinder. The spiral shape of the nanorod structures showed a relatively large solid fraction ratio value, and the values increased with increasing diameter of the spiral shape because the diameter of the spiral shape rather than the diameter of the nanorod was considered to be the diameter of the cylinder during image processing.

The WCAs of the fabricated GLAD nanostructures were measured and compared with the theoretically predicted values using the Cassie-Baxter model. Figure 2 illustrates the experimental and theoretical data of WCAs versus substrate rotation speed. The measured WCAs did not match the theoretical values when the substrate rotation speed was 0.2 rpm because of errors in estimating the diameter of the nanorods with a spiral shape. However, the measured WCAs of the GLAD nanorod samples prepared at a substrate rotation speed of 0.5 to 20 rpm were in a good agreement with theoretical values. As the f value was saturated when the substrate rotation speed was greater than 5 rpm, the WCA also saturated at about 138° for the samples prepared at a high rotation speed (>5 rpm). Based on this result, a substrate rotation speed of 5 rpm and a deposition rate of 10 Å/s were selected as the optimum processing conditions for the hydrophobic functional GLAD nanostructure because a high rotation speed might cause unexpected problems including vibration and detachment of the substrate during the deposition, and the fast deposition rate was advantageous in terms of fabrication cycle time.

3.2. Effects of Incident Angle on WCA. To examine the effects of incident angle on WCA, GLAD SiO_2 nanorod structures were fabricated with varying oblique angles (82°, 85°, and 87°) and a fixed nanorod height of 500 nm, a deposition rate of 10 Å/s, and a substrate rotation speed of 5 rpm. Figure 3 shows the top-view and cross-sectional SEM images of the GLAD nanostructures fabricated by varying the oblique angle (82°, 85°, and 87°). The data clearly show that that the increasing oblique angle increases the porosity of the surface, which significantly decreased the solid fraction ratio (f).

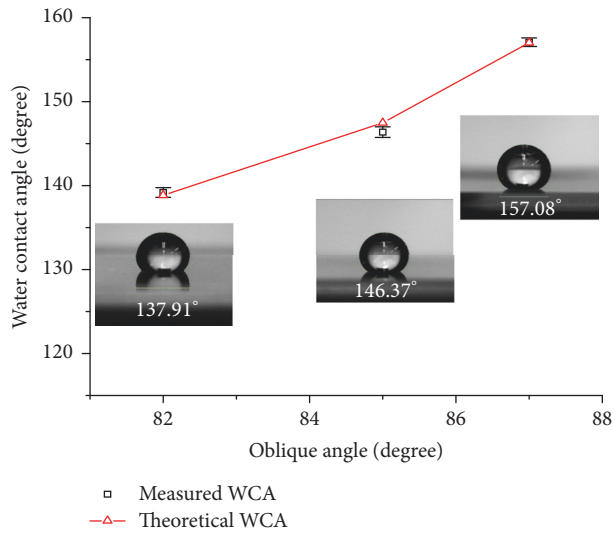

FIGURE 4: Effects of oblique angle on the measured and theoretical WCAs (Cassie-Baxter model) of GLAD nanorod substrates.

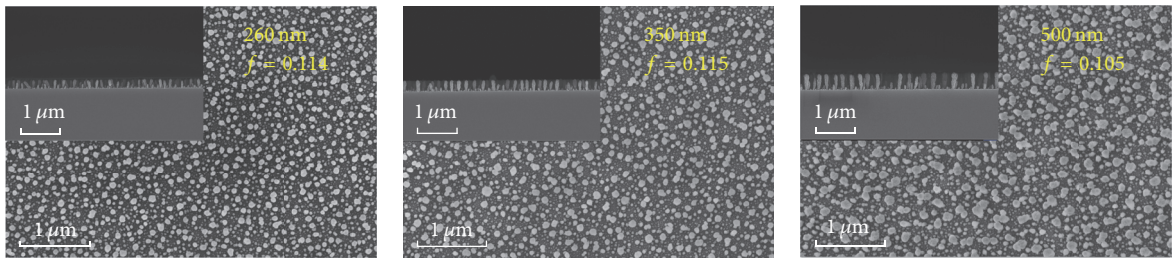

(a) (b) (c)

FIGURE 5: Top-view and cross-sectional view SEM images of fabricated GLAD SiO_2 nanorods with different heights of 260, 350, and 500 nm.

Figure 4 illustrates the measured and theoretical values of WCAs. As the oblique angle increased, the solid fraction ratio decreased, and the WCA increased. Since the GLAD SiO_2 nanorod structures used for Figure 3 were fabricated at a high rotation speed (5 rpm), they had a straight vertical shape, and the measured WCAs were in good agreement with the theoretical values. The highest contact angle of 157.08° was observed for columnar nanostructures fabricated at an oblique angle of 87°. Based on this result, the oblique angle of 87° was selected as the optimum processing condition.

3.3. Effects of Height of Nanorods on WCA and Optical Transmittance. To examine the effect of nanorod height on the WCAs, GLAD SiO_2 nanorods with different thicknesses of 260, 350, and 500 nm were fabricated at a 10 Å/s deposition rate, 5 rpm substrate rotation speed, and 87° substrate tilting angle. As shown in Figure 5, the diameter of the nanorods increased as the height of the nanorods increased, and the number of nanorods decreased. Therefore, the solid fraction ratios (f) were almost the same for all fabricated samples with different heights. Figure 6 shows the effects of the height of the nanorod on the measured and theoretical WCAs. As expected, the changes in WCA due to the changes in nanorod height were negligible.

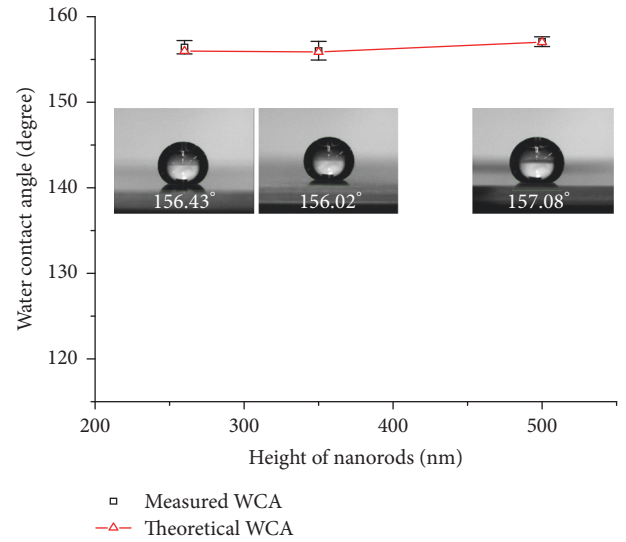

FIGURE 6: Effects of nanorod height on the measured and theoretical WCAs (Cassie-Baxter model) of GLAD nanorod substrates.

To confirm the optimal height of the nanorods for superhydrophobic functional nanostructured surfaces in optical applications, the optical transmission characteristics of the

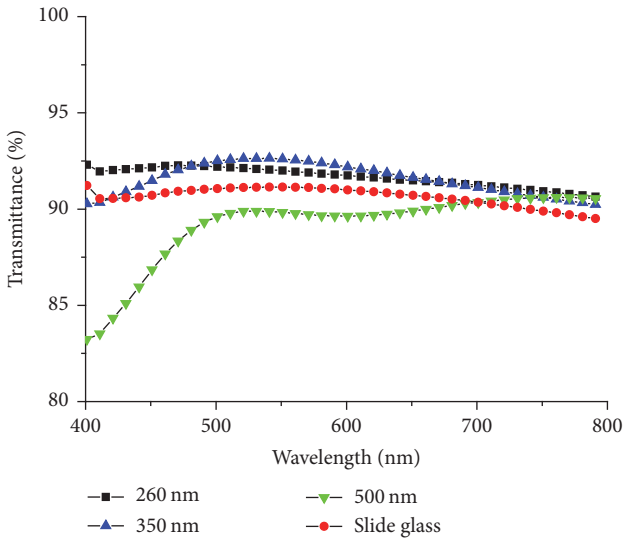

FIGURE 7: Light transmittance of the SiO_2 nanorod films with different thicknesses.

fabricated nanorods with different heights were measured as shown in Figure 7. The GLAD SiO_2 nanorod structures with thicknesses of 260 and 350 nm showed higher transmittance values than the conventional glass slide substrate in the visible range. However, the transmittance of GLAD SiO_2 nanorod structures at a height of 500 nm was lower than that of the glass slide substrate. This can be explained as follows. The taller nanorods had a larger diameter, and the 500 nm tall nanorods scattered the short-wavelength incident light because the transmittance was much lower at short wavelengths (400 to 500 nm). Based on these results, a nanorod height of 260 nm was selected in this study because the short nanorod structure was attractive from a fabrication cost perspective and provided good optical properties. The GLAD SiO_2 nanorod structure with a thickness of 260 nm prepared at a substrate rotation speed of 5 rpm, a deposition rate of 10 Å/s, and an oblique angle of 87° showed a WCA of 156.4° and ~2% higher light transmittance than the glass substrate in the whole visible range.

4. Summary and Conclusions

In this research, superhydrophobic (WCA of ~156°) and antireflection (~2% reduced reflection) functional SiO_2 nanorod structures were fabricated using the simple and inexpensive GLAD process. The GLAD nanorod structures fabricated at high substrate rotation speeds (>5 rpm) were considered circular pedestals, and the measured WCAs of the SiO_2 nanorods with a straight vertical shape well matched the theoretical WCAs from the Cassie-Baxter model. According to the Cassie-Baxter model, the WCA is related to the solid fractional ratio (f). The f value was not affected by the height of the nanorod or the deposition rate when the substrate rotation speed was faster than 5 rpm, but the f value was sensitive to the oblique angle. In this study, an oblique angle of 87° was selected to obtain the maximum water repellency. A substrate rotation speed of 5 rpm was chosen to generate straight vertical nanorods, and a deposition rate of 10 Å/s was used to minimize fabrication time. A nanorod height of 260 nm was selected to maximize the light transmittance because longer and larger nanorods are better at scattering incident light. Since the GLAD process can also be used for larger substrates, our on-going research is focused on solar cell cover glass production using the proposed GLAD nanorod structure fabrication process.

Conflicts of Interest

The authors declare that they have no conflicts of interest.

Acknowledgments

This research was supported by a grant from the Forensic Research Program of the National Forensic Service (no. NFS2017DNA05).

References

[1] A. Y. Al-hasan and A. A. Ghoneim, "A new correlation between photovoltaic panel's efficiency and amount of sand dust accumulated on their surface," *International Journal of Sustainable Energy*, vol. 24, no. 4, pp. 187–197, 2005.

[2] L. K. Verma, M. Sakhuja, J. Son et al., "Self-cleaning and antireflective packaging glass for solar modules," *Renewable Energy*, vol. 36, no. 9, pp. 2489–2493, 2011.

[3] X. Zhao, Q. Zhao, J. Yu, and B. Liu, "Development of multi-functional photoactive self-cleaning glasses," *Journal of Non-Crystalline Solids*, vol. 354, no. 12-13, pp. 1424–1430, 2008.

[4] K. Han, J. Shin, K. Kim, and H. Lee, "Nanosized structural anti-reflection layer for thin film solar cells," *Japanese Journal of Applied Physics*, vol. 50, no. 2R, p. 020207, 2011.

[5] T. Nishino, M. Meguro, K. Nakamae, M. Matsushita, and Y. Ueda, "The lowest surface free energy based on -CF3 alignment," *Langmuir*, vol. 15, no. 13, pp. 4321–4323, 1999.

[6] B. Bhushan, Y. C. Jung, and K. Koch, "Micro-, nano- and hierarchical structures for superhydrophobicity, self-cleaning and low adhesion," *Philosophical Transactions of the Royal Society A: Mathematical, Physical and Engineering Sciences*, vol. 367, no. 1894, pp. 1631–1672, 2009.

[7] A. Nakajima, "Design of a Transparent Hydrophobic Coating," *Journal of the Ceramic Society of Japan*, vol. 112, no. 1310, pp. 533–540, 2004.

[8] T. Aytug, J. T. Simpson, A. R. Lupini et al., "Optically transparent, mechanically durable, nanostructured superhydrophobic surfaces enabled by spinodally phase-separated glass thin films," *Nanotechnology*, vol. 24, no. 31, Article ID 315602, 2013.

[9] D. Öner and T. J. McCarthy, "Ultrahydrophobic surfaces. Effects of topography length scales on wettability," *Langmuir*, vol. 16, no. 20, pp. 7777–7782, 2000.

[10] B. Qian and Z. Shen, "Fabrication of superhydrophobic surfaces by dislocation-selective chemical etching on aluminum, copper, and zinc substrates," *Langmuir*, vol. 21, no. 20, pp. 9007–9009, 2005.

[11] D. K. Sarkar, M. Farzaneh, and R. W. Paynter, "Wetting and superhydrophobic properties of PECVD grown hydrocarbon and fluorinated-hydrocarbon coatings," *Applied Surface Science*, vol. 256, no. 11, pp. 3698–3701, 2010.

[12] C.-J. Ting, M.-C. Huang, H.-Y. Tsai, C.-P. Chou, and C.-C. Fu, "Low cost fabrication of the large-area anti-reflection films from polymer by nanoimprint/hot-embossing technology," *Nanotechnology*, vol. 19, no. 20, Article ID 205301, 2008.

[13] D. P. Singh and J. P. Singh, "Controlled growth of standing Ag nanorod arrays on bare Si substrate using glancing angle deposition for self-cleaning applications," *Applied Physics A: Materials Science and Processing*, vol. 114, no. 4, pp. 1189–1193, 2014.

[14] S. Kumar, P. Goel, D. P. Singh, and J. P. Singh, "Highly sensitive superhydrophobic Ag nanorods array substrates for surface enhanced fluorescence studies," *Applied Physics Letters*, vol. 104, no. 2, Article ID 023107, 2014.

[15] S. Bruynooghe, D. Tonova, M. Sundermann, T. Koch, and U. Schulz, "Antireflection coatings combining interference multilayers and a nanoporous MgF_2 top layer prepared by glancing angle deposition," *Surface and Coatings Technology*, vol. 267, pp. 40–44, 2015.

[16] S. Chhajed, M. F. Schubert, J. K. Kim, and E. F. Schubert, "Nanostructured multilayer graded-index antireflection coating for Si solar cells with broadband and omnidirectional characteristics," *Applied Physics Letters*, vol. 93, no. 25, Article ID 251108, 2008.

[17] S. Kim, W. Zhang, and B. T. Cunningham, "Coupling discrete metal nanoparticles to photonic crystal surface resonant modes and application to Raman spectroscopy," *Optics Express*, vol. 18, no. 5, pp. 4300–4309, 2010.

[18] Y.-P. Zhao, D.-X. Ye, G.-C. Wang, and T.-M. Lu, "Novel nano-column and nano-flower arrays by glancing angle deposition," *Nano Letters*, vol. 2, no. 4, pp. 351–354, 2002.

[19] Y.-A. Han, J. Ju, Y. Yoon, and S.-M. Kim, "Fabrication of cost-effective surface enhanced raman spectroscopy substrate using glancing angle deposition for the detection of urea in body fluid," *Journal of Nanoscience and Nanotechnology*, vol. 14, no. 5, pp. 3797–3799, 2014.

[20] M. Suzuki, "Practical applications of thin films nanostructured by shadowing growth," *Journal of Nanophotonics*, vol. 7, no. 1, Article ID 12150SSP, pp. 073598-073598, 2013.

[21] R. N. Wenzel, "Surface roughness and contact angle," *The Journal of Physical Chemistry*, vol. 53, no. 9, pp. 1466-1467, 1949.

[22] A. B. D. Cassie and S. Baxter, "Wettability of porous surfaces," *Transactions of the Faraday Society*, vol. 40, pp. 546–551, 1944.